DEPARTMENT OF PHYSICS

Characterizing CEPA

a phoswich array

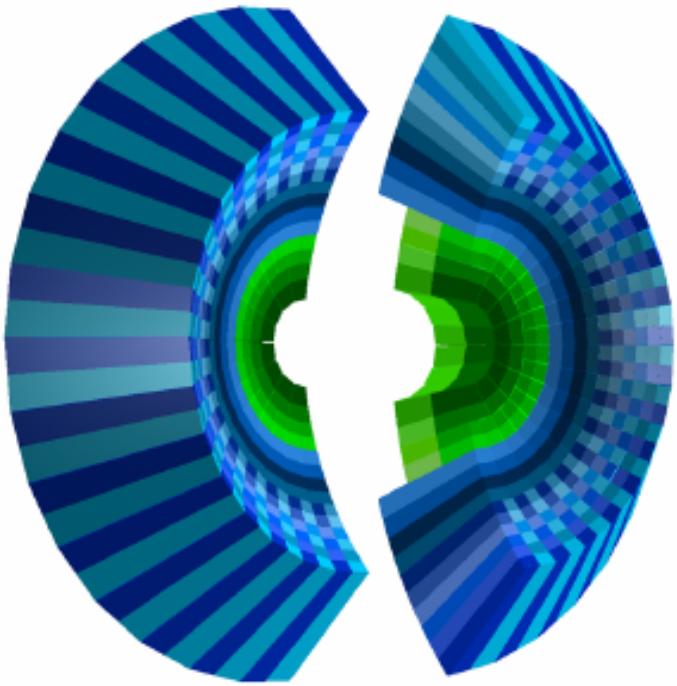

Yusuf Ali
Valdemar Bergentall
Erik Dahlgren

Degree project for Bachelor of Science with a major in Physics
Gothenburg, Sweden 2019,
180 HEC, First Cycle

Bachelors's thesis 2019

Characterizing CEPA a phoswich array

Investigation of certain characteristics of one sector of the CEPA detector

Yusuf Ali
Valdemar Bergentall
Erik Dahlgren

Department of Physics
Gothenburgs University
Gothenburg, Sweden 2019

Characterizing CEPA
a phoswich array

Supervisors: Håkan T Johansson & Andreas Heinz
Examiner: Martina Ahlberg

Bachelor's Thesis 2019
Department of Physics
Gothenburgs University
SE-412 96 Gothenburg
Telephone +46 31 772 1000

Cover: Artistic picture of the CEPA-detector.

Typeset in LaTeX
Gothenburg, Sweden 2019

Abstract

The structure of unstable nuclei is studied at the international facility FAIR, Darmstadt, Germany. One experimental setup at FAIR is called R^3B where radioactive beams at relativistic energies impinge on a specific target which allows to collect data on the reactions taking place. For these experiments, different detectors have been built and CEPA is one of them. CEPA is the detector that will be characterized in this thesis. This detector consists of 24 sectors, where each sector has four tightly packed scintillator detectors, each a combination of $LaBr_3$ and $LaCl_3$, making up a phoswich crystal unit. Each phoswich crystal unit is made out of 7 cm $LaBr_3$ and 8 cm $LaCl_3$, respectively. Previous CEPA prototypes have been characterized at Chalmers, but the latest CEPA crystals have a new geometrical shape, the shape of a frustum. The three characteristics of CEPA that are investigated are their energy calibration, their energy resolution and the dependence of the detected energy on the position of the interaction. It was found that the energy resolution for the four $LaBr_3$ parts of the tested sector did not meet the requirements [5]. Crystal one was the closest to meet the requirements, but still did not met the requirements with a factor 1.73 times higher (resolution) compared with the prototype, the other crystals were approximately a factor 2.5 higher. On the $LaCl_3$ part none of the crystals met the requirements. The calibration measurements were also not successful since the characterized peak positions for different γ-sources did not end up on the expected place for all the sources. Unfortunately the sector that was investigated exhibited a significant position dependence.

Sammanfattning

Strukturen av ostabila atomkärnor studeras vid den internationella anläggning FAIR (Facility for Antiproton and Ion Research) i Darmstadt, Tyskland. En av experimentuppställningarna vid FAIR är R^3B (Reactions with Relativistic Radioactive Beams), där man accelererar radioaktiva isotoper och bombarderar ett target. För att kunna analysera den värdefulla datan som kommer från dessa reaktioner har det byggds ett flertal detektorer. CEPA är en av detektorerna och den har studerats i detta arbete. CEPA är uppdelad i 24 sektorer där varje sektor består av fyra packade scintillator-detektorer. Varje scintillatordetektor är uppbyggd av sju cm $LaBr_3$ och åtta cm $LaCl_3$. Tidigare CEPA-prototyper har testats på Chalmers. Det som skiljer protyperna från de nya detektorerna är den geometriska formen. De nya detektorerna är kilformade. Det är tre egenskaper som har studerats i detta arbete: kalibrering, enegiupplösning och positionsberoende. Energiupplösningen för CEPA-sektorns $LaBr_3$-del uppfyllde inte kraven [5], endast kristall 1 var i närheten av de tidigare resultaten med en faktor 1,73 högre upplösning än prototyperna. De övriga kristallerna hade en energiupplösning ungefär 2,5 gånger högre än prototyperna. För $LaCl_3$-delen av sektorn så uppfylldes inte kraven för någon kristall. Kalibreringen för sektorn var inte heller lyckad då topp-positionerna inte stämde överens med de förväntande värdena. Sektorn har även ett positionsberoende vilket inte är bra.

Keywords: CALIFA, CEPA, Phoswich, $LaBr_3$, $LaCl_3$, Energy resolution.

Acknowledgements

First of we want to thank Håkan T. Johansson and Andreas Heinz for giving us the opportunity to work on this project. Furthermore we want to thank Andreas Heinz for his unlimited knowledge in experimental nuclear physics and his preciseness. Håkan T. Johansson for his great input in both analyzing the data and in overall nuclear theory, and also for his "to do it" attitude. Finally we also want to thank Giovanni Bruni and Paloma Diaz Fernandez for their assistance in understanding the scripts used in this report and also for valuable information about CEPA4.

Valdemar Bergentall,
Erik Dahlgren,
Yusuf Ali

Contents

1
Introduction

1.1 Introduction

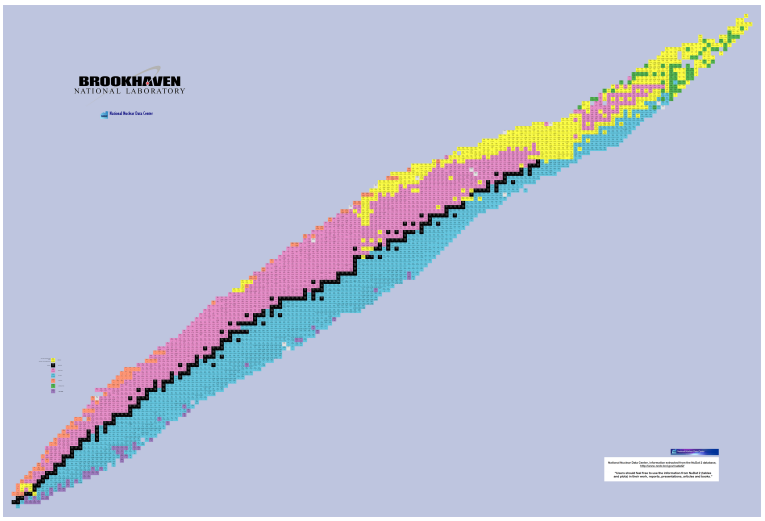

Figure 1.1: The chart of nuclides, where the y-axis represents the number of protons and the x-axis the number of neutrons. Black squares represent stable nuclei, blue are nuclei decaying through β^- decay, pink nuclei decays via β^+ or electron capture, yellow squares represents alpha decay, green spontaneous fission, orange proton emission, and purple squares indicate neutron emission [3].

A key role of nuclear physics is to understand atomic nuclei and thier structure. The constituents of nuclei, protons and neutrons are interacting by different types of forces: the strong force, the weak force and the electromagnetic force. All these forces play a role in determining the structure and the decay of nuclei. Atomic nuclei which are not stable are studied for example at FAIR (Facility for Antiproton and Ion Research) in Darmstadt, Germany.
A way of understanding new properties of nuclei is to study the extreme state, in this case reach and go beyond the drip lines for both protons and neutrons. Drip-lines define where the nuclei are no longer bound when more protons or neutrons are added. In other words, inside the drip-lines, unstable nuclei decay by the weak force (β-decay). Outside the drip-lines, unstable nuclei are not held together by the strong force. Another way of obtaining information on nuclear structures is based on reaction studies with relativistic radioactive beams and stable targets. One

such measurement is called R^3B (Reactions with Relativistic Radioactive Beams) at FAIR. It uses a beam of radioactive ions of any element of interest, which is focused towards a stable target, the target could be any type of element. The products that are created in these reactions are measured by different types of detectors. The use of radioactive beams gives scientists access to about 3000 different isotopes to investigate. One of the detectors used at R^3B is CALIFA (CALorimeter for the In-Flight detection of γ rays and light charged pArticles.) It is positioned around the target. CALIFA will be able to detect protons with a large range of energies, while also characterizing gamma photons with a good energy resolution. CALIFA will be able to measure the 4-momenta of those reaction products [1]. The CALIFA detector is divided into three different parts, the Barrel, IPHOS (Intrinsic PHOSwich detector) and CEPA (Califa Endcap Phoswich Array), see Figure 1.2 [4].

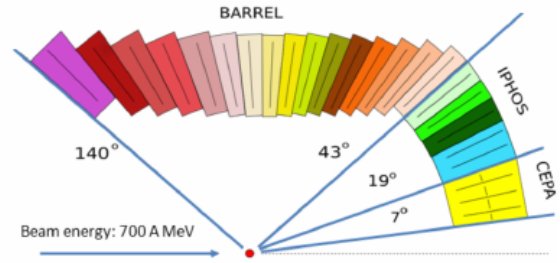

Figure 1.2: The CALIFA detector is divided into two main parts, the Barrel and the Forward EndCap. The EndCap is further subdivided into IPHOS and CEPA.

The barrel takes up most of the solid angle and CEPA the least. In this thesis we will focus on the CEPA detector. CEPA consists of 24 sectors, the geometry of a sector is a frustum and each sector consists of four crystals. Each crystal uses the phoswich technique which will be explained in section 2.1. The sectors are enclosed in a two millimeter aluminum casing.

1.2 Background

While an investigation of a previous prototype of CEPA has been performed before [4], the geometric shape of the crystals for the final sectors has changed, measurements are required to see if any crucial property of the sectors is different, and if so, to try to determinate if that is related to the manufacture process. The TDR (Technical Design Report) [5] for the CALIFA project defines the requirements for e.g. the energy resolution that each detector element has to meet. In this thesis we focus on measurements that involve gamma-photons, to determinate energy resolution and position dependence. Because the measurements are done using natural γ-sources, there is no need for a pulse shape analysis, since no natural gamma source is capable of providing γ-rays, which penetrate the layer of $LaBr_3$ or $LaCl_3$ crystals. The task is to check if the crystals are of sufficient quality to be used in the experiment.

1.3 Hypothesis

Since prototypes of the crystals made from the same scintillator materials have been manufactured and tested before, namely CEPA4, and only the geometric structure has been changed, we expect the new crystals to have a similar energy resolution to CEPA4. Also since the CEPA4 crystals showed almost no position dependence of the measured energy, we expect to see the same in the new crystals. The company Saint Gobain is the manufacturer of the crystals of CEPA4 and of the crystals to be investigated in this work.

2

Method

This section presents the experiment setup, the instruments used in the the measurements and the method for characterizing the three characteristics of the crystals, the energy resolution, the calibration and the position dependence. The data collection and analysis method is also presented.

2.1 Instruments

Below instruments used in the measurements are described. The intruments mentioned are the phoswich crystals, PMT and the digitizer CAEN.

2.1.1 Phoswich detectors and scintillator crystals

Phoswich detectors are a up-coming instrument in nuclear physics, often used to mesure the energy deposit of particles in different scintillator materials. What makes a phoswich detector special is that it is composed of multiple scintillator materials, in our case two, that are connected to the same photomultiplier tube. The drawback with the phoswich technique is that the two signals have to be disentangled. Therefore pulse-shape analysis needs to be performed and by using the fact that the two scintillator materials have different time constant, the signal can be disentangled. The advantage is that the total energy of the particle can be extracted without the particle stopping in the the detector. The two scintillator materials used are lanthanum bromide ($LaBr_3$) and lanthanum chloride ($LaCl_3$). $LaBr_3$ is positioned at the front of the sector infront of the $LaCl_3$ crystal. Both $LaBr_3$ and $LaCl_3$ are inorganic scintillator materials, which scintillate due to optical transitions in their band structure. The main reason why scintillators are used is because of the good intrinsic energy resolution of $LaBr_3$ and $LaCl_3$ crystals, together with their high stopping powers for protons. $LaCl_3$ is chosen because it is transparent to the light of $LaBr_3$. Both have short decay constants, $LaBr_3$ has 16 nanoseconds and $LaCl_3$ 28 nanoseconds. Both of the scintillators have a fast rising time of around 5 ns. This means that the pulse-shape analysis of the combined pulse is easier to analyze since the rising times are the same, while the different decay times allow to distinguish the pulses.

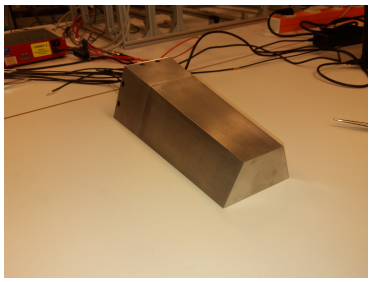

(a) Picture of the sector that is investigated in this project.

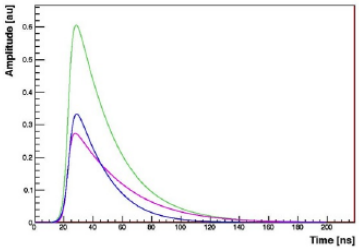

(b) Pulse shaper for $LaBr_3$ and $LaCl_3$. Purple represents the $LaCl_3$ crystals, blue the $LaBr_3$ and green shows the combined pulse.

Figure 2.1: Picture of a sector of CEPA crystals and the pulse from each scintillator and the combined pulse.

2.1.2 Photomultiplier tube, PMT

The function of the photomultiplier is to convert a single or a few photons, into a measurable current. The energy of the photons from the γ-sources is absorbed in the scintillators, exciting thier electrons, which on de-excitation, emit new photons in the optical range. When these photons hit the photocathode in the photomultiplier it produces free electrons by the photoelectric effect. The electrons are accelerated by the electric field from the high voltage feeding to the dynodes. The dynodes then liberate more electrons from their material when they are struck by the incoming electrons. This is called secondary emission. The gain is exponential and this effect carries through to the other dynodes. When dynodes are coupled together they produce enough electrons for a strong current/signal [6], see Figure 2.2 and Figure 2.3 where it can be seen that the PMT gain is exponential.

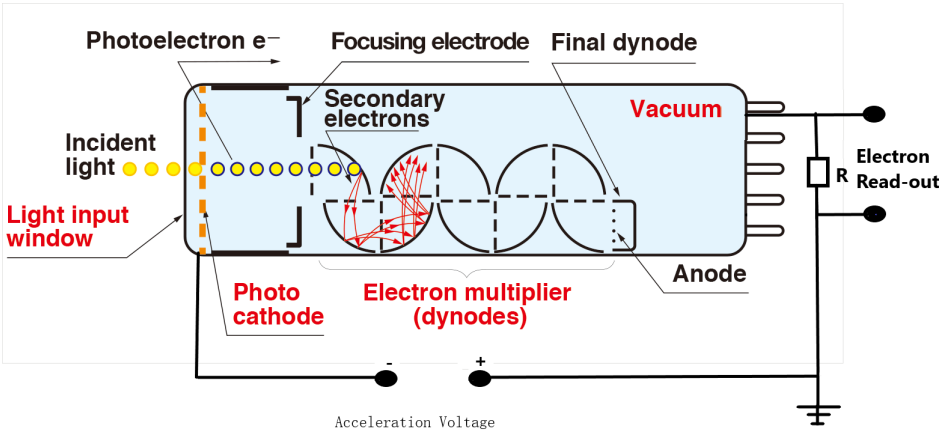

Figure 2.2: Schematic drawing of a photomultiplier [6].

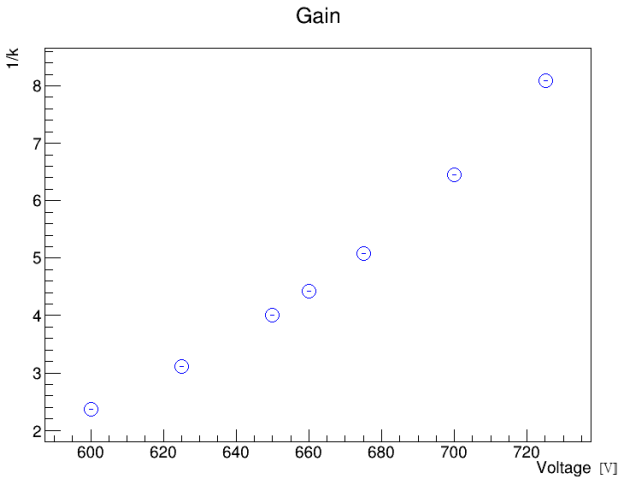

Figure 2.3: The gain is exponential when a higher voltage is applied as expected. The y-axis describes the gain as $1/k$, were k is the linear slope of ^{22}Na.

2.1.3 CAEN digitizer

A digitizer collects analog information, in our case as light and then transforms it to digital information as a text file. In all measurements a digitizer, CAEN DT5730, was used. The DT5730 has an input voltage range of $2V$ peak-to-peak, a resolution of 14 bits and a sampling frequency of 500 MHz. It has a built-in software, which allows to change parameters during measurements. Is is also possible to ignore certain signals from specific crystals if desired. An editable configuration file is available, however for the measurements in this project the same configure file of the CAEN has been used.

2.1.4 γ-sources

Four sources were used to test the crystals: ^{22}Na, ^{60}Co, ^{137}Cs as well as room background radiation that can have traces of ^{40}K. The half-lives for the sources are 2.602, 5.27 and 30.17 years, respectively.

2.2 Experimental setup

During the measurements (energy resolution) performed in this work the source was placed in front of the crystal. Different PMT voltages were tested, as well as different positions of the source and different sources.

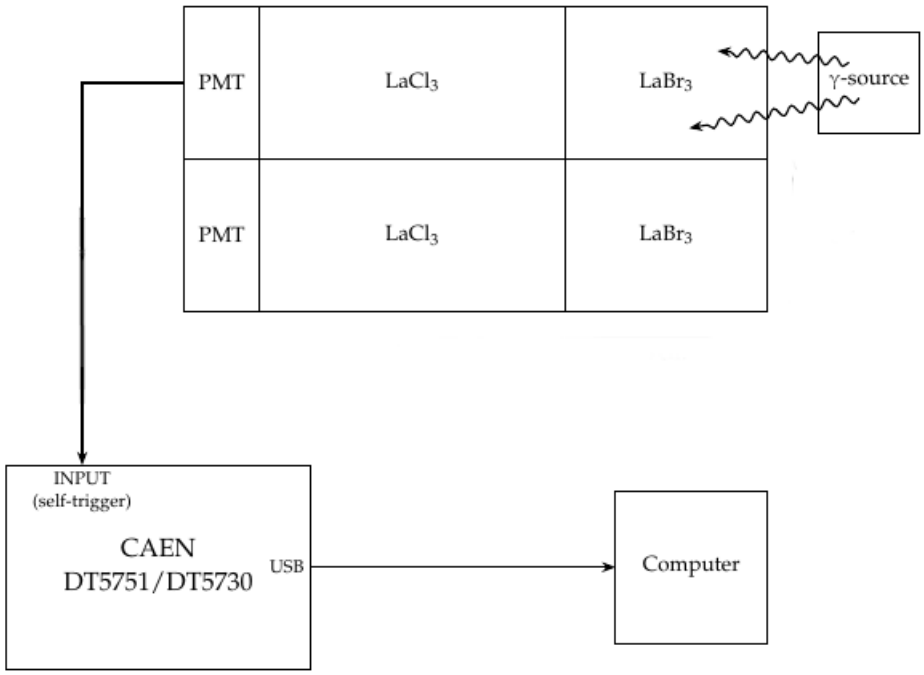

Figure 2.4: A schematic illustration of the setup used in the measurements.

2.2.1 Energy resolution of CEPA crystals

The energy resolution was the first characteristics of the CEPA crystals that was investigated. The resolution itself is determined from a Gaussian fit on the measured peaks. The width of the peak is given by the definition of a Gaussian curve :

$$f(E) = A \cdot e^{(-E-\bar{E})^2/2\cdot\sigma^2} \tag{2.1}$$

where A is the normalization factor of the peak amplitude and E its energy, in our case its the peak energy. For $f(E_1) = f(E_2) = A/2$, two different points on the curve equal half of the amplitude. The energy difference is related to σ by

$$E_2 - E_1 = \Delta E = 2 \cdot \sigma\sqrt{2 \cdot ln2} \cong 2.35\sigma, \tag{2.2}$$

and is called the Full Width Half Maximum (FWHM)[2]. The FWHM is frequently used when describing the energy resolution. In order to obtain the relative energy resolution, the FWHM needs to be divided by $\bar{x}$, which is the mean peak position. In this thesis every time a energy resolution is mentioned it is given as relative energy resolution based on the FWHM.
One important requirement of the CEPA crystals is their energy resolution. The second peak of a ^{60}Co source (1332.49 keV) should have a resolution better than

Figure 2.5: Picture of back end of Sector 1, where one can see the cables connected to the different crystals.

2.5%[5]. Different positions of the source were tested to see if the resolution had any position dependence. Fig. 2.6 shows the front face of the tested detector module and the placement of the γ-sources used.

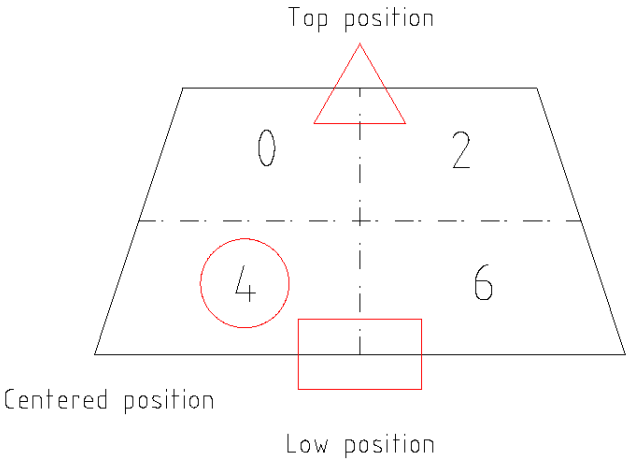

Figure 2.6: The schematic of the front face of a sector, the four crystals, labeled 0, 2, 4 and 6 (the channels) and the three positions where the source was placed.

2.2.2 Position dependence

Position dependence of the detector signal is the second detector property that was investigated in this project. Ideally this means that the position of the peak in the spectrum should be at the same place wherever the gamma photons interact, which can be tested using different source positions.
The two approaches to do these measurements are the "centerline" method and with a collimator. The "centerline" method is to place the source on top of the crystal which will increase the spread of photons in the crystal and the distance between the source and crystal is around 5 mm. To do this a "centerline" is defined between the different channels, wherein top "centerline" is where channels 0 and 2 are investigated and bottom "centerline" is for channels 4 and 6. To get a sufficient number of datapoints for both the $LaBr_3$ and the $LaCl_3$ of the crystal a distance of 10 mm between each measurement along the "centerline" is set.

The other method is based on using a collimator. The purpose of the collimator is to provide a more defined view where the photons interact in the detector. The collimator (see figure 2.8) is made of lead and is 5 cm thick, the radius of the hole for the incoming photons is 11 mm and the outgoing hole is 6 mm, the hole changes its radius approximately halfway through the collimator.

Before the measurements were performed, simulations were done with "GGLAND" which is a wrapper for the GEANT4 data library. In these simulations we compared what difference it would be if we used a collimator versus no collimator.

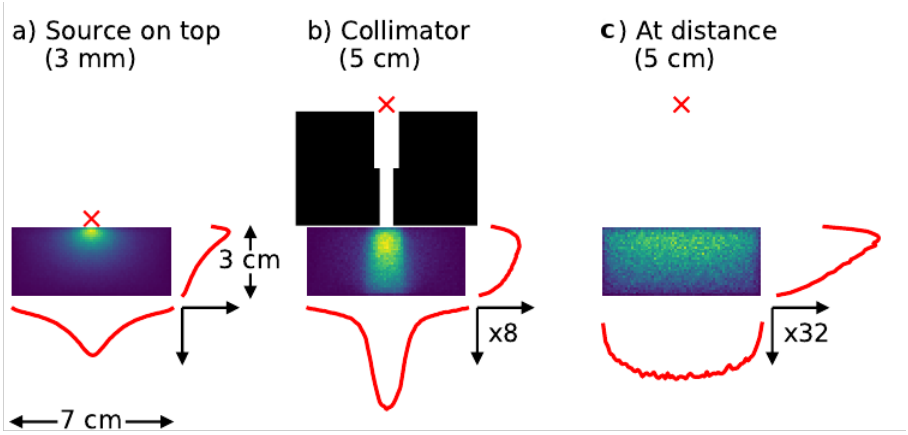

Figure 2.7: Figures from three different simulations. Blue space equals no interaction of photons and the brigther the yellow the more interactions. The red curve below each figure is an approximation of what the peak in the spectrum would look like, the (x8) and (x32) represents the amount of time needed to get the same statistics as in the first figure (a).

As can be seen from the simulations in Fig. 2.7 the interaction depth in the crystal is much more defined when using a collimator, as expected. Also to get similar results as when using no collimator as in Fig. 2.7 a) the length of the measurement were increased by a factor of 8, this is not only because of that the spread of the

photons is more defined, but the gamma source is placed further away which leads to a decrease in counts, seen in Fig. 2.7 (c). It also shows that there is no possibility to determine where specific photons actually interacted.
To perform measurements a rig was constructed with Lego-bricks and some plexiglas (Fig. 2.8). Beneath the crystal there is a support structure, so the surface of the crystal that is investigated will always be flat, the other Lego-bricks work as pillars to place a plexiglas layer on top of the detector. On the plexiglas we placed the collimator. Since the collimator is formed as a cube, a paper that is marked with numbers indicates the position of the outgoing hole, so the results can later be compared with the "centerline" method. One final important detail when using the collimator, is that the distance between the plexiglas and the crystal is 1 cm. This results in a distance of approximately 6 cm between the crystal and the γ-source when using the collimator.

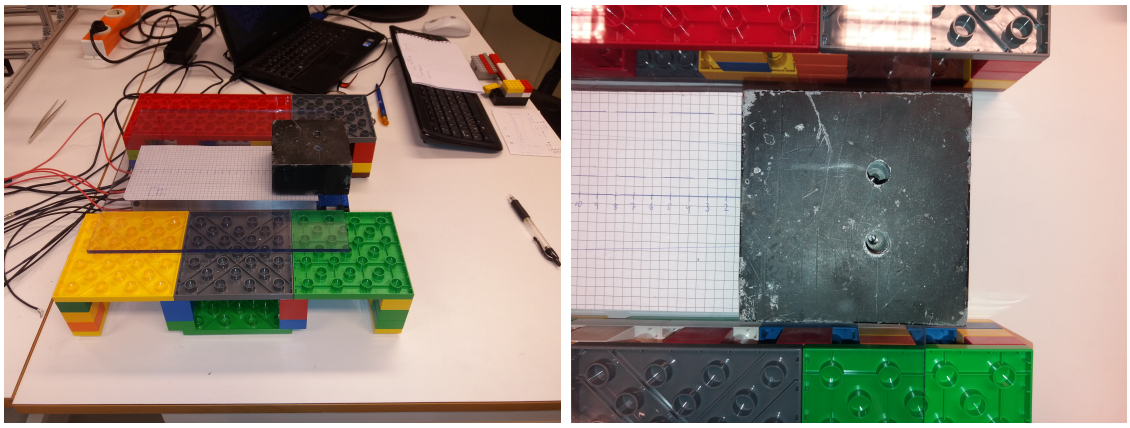

Figure 2.8: Pictures of the collimator, a side view and a view from above. They also show the paper which indicates where the hole for outgoing photons is positioned. Note that the detector is arranged beneath the collimator and the paper in the pictures. For more pictures of the setup see Appendix A.

2.3 Data collection & analysis methods

Here the scripts used in the work is described and also methods how we get a spectrum from the signals obtained from the digitizer.

2.3.1 Scripts

A script by the name "energyReconstuction", that can read text files storing the digital information from the digitizer, was written built through a number of exercises from the supervisors. The text files we used had sizes of around 1 GB and consisted of around 500 000 events with 300 samples each. One event corresponds to one pulse from the crystal. The script calculates the integral between two limits, which includes the pulse. The resulting values are later put into a histogram where the gamma peaks of interest are visible. Thereafter the script uses the peak finding function Tspectrum of ROOT[1] to find the positions of the peaks. This script was used mainly for calibration purposes.

The second script is called "enResBasic" which does the same thing as energyReconstruction but has more options to extract resolution and similar tasks. enResBasic calls on a larger script "readCaenFile" with a lot of structures. The major calculations are performed in readCaenFile and the the figures are created by enResBasic. The procedure of the fitting in the script readCaenFile follows, first a Gaussian fit to the peaks is done, then a linear fit is applied to project the Gaussain fit on the x-axis.

2.3.2 Baseline

Signals from the PMTs are shaped as pulses. The first analysis done on the raw data is a calculation of the baseline, which is defined as the mean of the first twenty samples of each pulse. This ensures that no part of the actual pulse contributes to the baseline, which was checked by inspecting signal traces. There is no need to check this (manually) since the digitizer has a tool called pre-trigger, which determines how many samples the digitizer takes into account before the pulse begins.

[1] CERNs own analysis framework that has been developed since 1997 for handling big data and statistical analysis. It is mainly coded in C++.

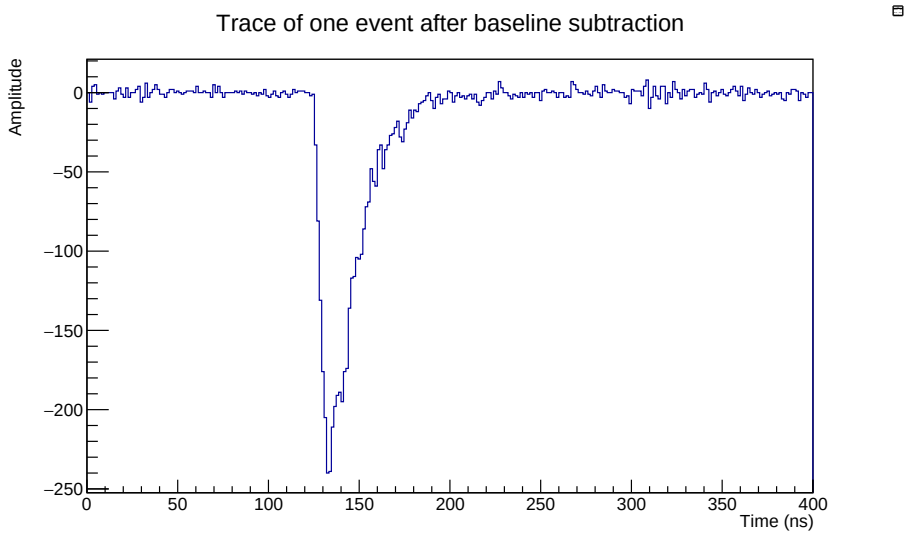

Figure 2.9: The trace from of LaBr crystal after the baseline is subtracted. On the y-axis the amplitude is given in a.u.

Knowledge of the baseline is needed because the output data from the photomultiplier contains electronic noise, which can be reduced by a baseline subtraction.

2.3.3 From pulses to spectra

When the pulses are "clean" some analysis can be done to get the best possible result. To obtain a spectrum from of the pulses, a script is used to calculate the area of each pulse and store the areas in a histogram. When calculating the area, one can optimize. Not all of the baseline needs to be included in the integration.

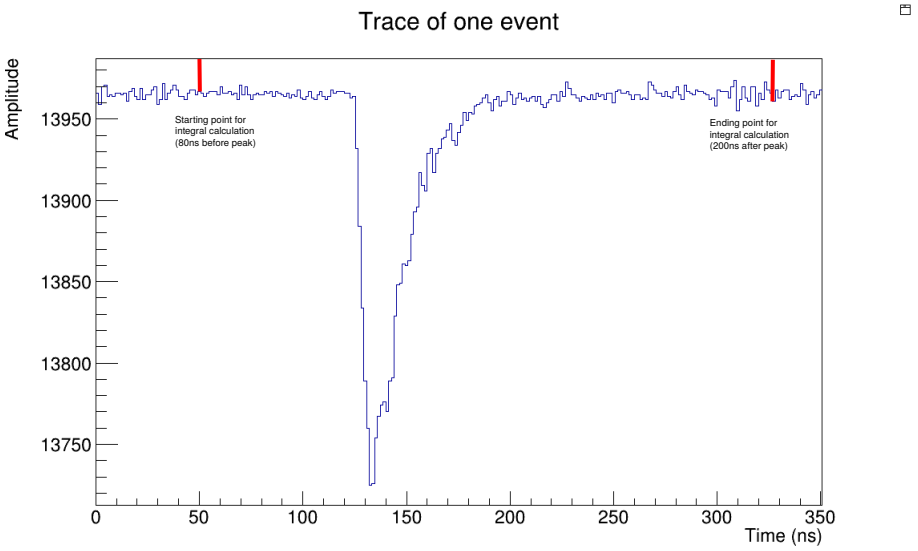

Figure 2.10: Trace from the LaBr part where the red lines indicate the limits for the integral calculation. On the y-axis the amplitude is given in a.u. Note that the baseline is not subtracted from the pulse here.

Different limits for the pulses were investigated to see their impact on the final energy resolution. First a fixed limit after the peak position of the pulse was set and the limit before the peak position differed, when the lowest energy resolution value is found, that value is fixed and the limit for the tail is varied until the best limits were found. A value of 40 ns before and 100 ns after the peak position for the LaBr, and 40 ns and 150 ns for the LaCl, respectively gave the best results The limits do not have a great impact on resolution which can be seen in Ref [4].

2.4 Calibration

To transform the uncalibrated data in energy channels into a calibrated spectra in keV, a calibration is needed. There is a linear correlation between these two spectrums, through the equation

$$y = kx + m. \tag{2.3}$$

The slope "k" is calculated through

$$k = \frac{\Delta y}{\Delta x} = \frac{y_2 - y_1}{x_2 - x_1} \tag{2.4}$$

were y is the tabulated peak position for the isotope, see table 2.1, and x is the peak position in energy channels. For a calibration, two peaks are needed from the source, e.g the two peaks in ^{22}Na, which are 511.1 and 1274.537 keV, then the peak position is acquired from the measurement and script. One example of this, is a calibration of ^{22}Na

$$\frac{511.1 - 1274.537}{4112.10225 - 10274.48168} = 0.123887 \tag{2.5}$$

The offset is calculated either through

$$m = y_1 - k \cdot x_1 \tag{2.6}$$

or

$$m = \frac{x_1 y_2 - x_2 y_1}{x_1 - x_2} \tag{2.7}$$

which gives the same value for m. Examples of a calibrated and an uncalibrated spectra are presented in figure 2.11.

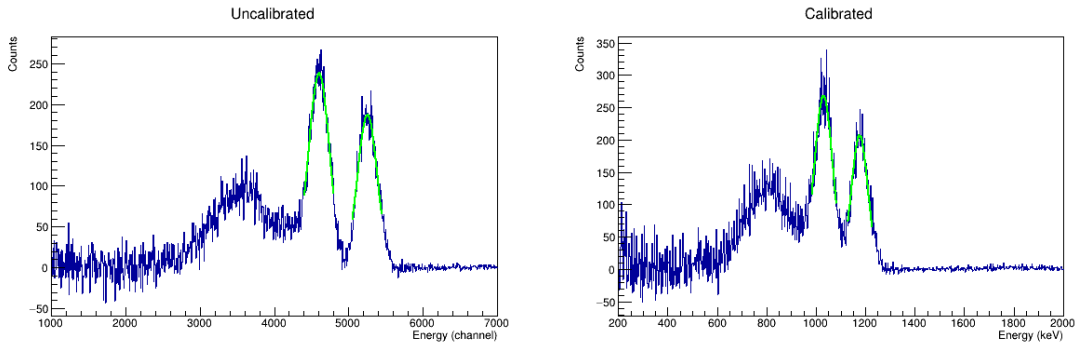

(a) uncalibrated data

(b) calibrated data

Figure 2.11: Example of a spectrum before and after calibration for ^{60}Co .

2.4.1 Uncertainty of the measurements

It is apparent that all experimental measurements have uncertainties. This means that the k- and m- values, where k is the slope and m is the offset calculated from

the linear equation (2.3), will also contribute an amount of uncertainty, ∂k and ∂m respectively. These uncertainties can be given as a value that is either added to or subtracted from the measurement as shown in table 2.3.

Assume that the resultant R, is a function of variables from x_1 through x_n, as shown in equation (2.8).

$$R = f(x_1, x_2, x_3, ...x_n) \tag{2.8}$$

Then the uncertainty represented by σ_R of the resultant R is a function of the uncertainties of all of those variables.

$$\sigma_R = f(\sigma_{x_1}, \sigma_{x_2}, \sigma_{x_3}, ...\sigma_{x_n}) \tag{2.9}$$

The uncertainty of R is given by the root sum of the squares so called (RRS) of the partial derivative of each variable multiplied by the variable's uncertainty as shown below in equation (2.10).

$$\sigma_R = \pm\sqrt{\sigma_{x_1}^2 \cdot \left(\frac{\partial R}{\partial x_1}\right)^2 + \sigma_{x_2}^2 \cdot \left(\frac{\partial R}{\partial x_2}\right)^2 + \sigma_{x_3}^2 \cdot \left(\frac{\partial R}{\partial x_3}\right)^2 + ... + \sigma_{x_n}^2 \cdot \left(\frac{\partial R}{\partial x_n}\right)^2} \tag{2.10}$$

2.4.1.1 Propagation of uncertainty

In the case of error propagation within linear systems, one can solve k- respectively m- value from equation 2.3 where k is the slope and m is the offset by:

$$k = \frac{\Delta y}{\Delta x} = \frac{y_2 - y_1}{x_2 - x_1} \quad \text{and} \quad m = \frac{x_1 y_2 - x_2 y_1}{x_1 - x_2} \tag{2.11}$$

This linear equation was rewritten to:

$$y = k(x - x_0) + m_0 \quad \text{where} \quad x_0 = \left(\frac{x_1 + x_2}{2}\right) \tag{2.12}$$

The reason for creating the variable x_0 was the fact that sodium peaks (511.1 and 1174.5 [keV]), which were used in the calibration, are located far away from each other. The idea is to find a value that lies midway between these two peaks and thereby take an average of them and call it x_0.

Furthermore, we have the possibility to calculate ∂y with respect to k and m_0 respectively from equation (2.12) in order to be able to subsequently solve on ∂k and ∂m from it and use it in equation (2.18) when calculating the total uncertainty.

$$\Rightarrow \begin{cases} \frac{\partial y}{\partial k} = (x - x_0) \\ \frac{\partial y}{\partial m_0} = 1 \end{cases} \tag{2.13}$$

From equation (2.11), we can express ∂k with respect to x_1 and x_2 in order to calculate the uncertainty that lies in the slope by:

$$\left(\frac{\partial k}{\partial x_1}\right)^2 = \frac{y_2 - y_1}{(x_2 - x_1)^2} \quad \text{and} \quad \left(\frac{\partial k}{\partial x_2}\right)^2 = -\frac{y_2 - y_1}{(x_2 - x_1)^2}. \tag{2.14}$$

Solving ∂k from equation 2.14, gives:

$$\partial k = \pm\sqrt{(\partial x_1^2 + \partial x_2^2)\left(\frac{y_2 - y_1}{(x_2 - x_1)^2}\right)^2} \tag{2.15}$$

where ∂k is the uncertainty that lies in the slope, x_1 & x_2 are the peak energies in [bins], y_1 & y_2 are the peak energies in [keV] from nndc [7] and ∂x_1 and ∂x_2 respectively are the uncertainties of the calibrated sodium peaks calculated by ROOT. See Table 2.4.

By using the previous principle of calculating the uncertainty of the slope, we were now able to use it to calculate the uncertainty in the offset. Note that equation (2.11) is used again also in this case.

$$\left(\frac{\partial m}{\partial x_1}\right)^2 = x_2\frac{y_2 - y_1}{(x_2 - x_1)^2} \quad \text{and} \quad \left(\frac{\partial m}{\partial x_2}\right)^2 = x_1\frac{y_2 - y_1}{(x_2 - x_1)^2}. \tag{2.16}$$

Furthermore, from equation (2.16), we get:

$$\partial m = \pm\sqrt{\partial x_1^2 \cdot \left(\frac{x_2(y_1 - y_2)}{(x_1 - x_2)^2}\right)^2 + \partial x_2^2 \cdot \left(\frac{x_1(y_2 - y_1)}{(x_1 - x_2)^2}\right)^2} \tag{2.17}$$

where ∂m is the uncertainty that lies in the offset and remaning parameters are the same as in equation (2.15).

Finally, we use equation (2.18) below to calculate the total uncertainties in the whole system. In this case we have a combination of ^{137}Cs and ^{22}Na to calculate it. What we mean by a combination of ^{137}Cs and ^{22}Na is that we simply use the energy peaks from the respective sources.

∂k^2 & ∂m^2 which are the uncertainties in the slope and offset respectively were calculated from equation (2.15) and (2.17), as well as $\left(\frac{\partial y}{\partial k}\right)^2$ & $\left(\frac{\partial y}{\partial m_0}\right)^2$ and $R_{uncertainty}$ is the uncertainty from the calibration which lies in ^{137}Cs calculated by ROOT.

See Table 2.2 and 2.4 to keep track of the values used in the upcoming equation (2.20).

$$\sum_{\text{total uncertainty}} = \sqrt{\partial k^2 \cdot \left(\frac{\partial y}{\partial k}\right)^2 + \partial m^2 \cdot \left(\frac{\partial y}{\partial m}\right)^2 + \mathrm{R}^2_{\text{uncertainty}}} \quad \text{[keV]} \tag{2.18}$$

$$= \sqrt{\partial k^2 \cdot \left(\frac{y - m_0}{k}\right)^2 + \partial m^2 \cdot 1 + \mathrm{R}^2_{\text{uncertainty}}} \tag{2.19}$$

$$= \sqrt{0.000167 \cdot \left(\frac{661.657 - 892.8185}{0.263842}\right)^2 + 0.241463 \cdot 1 + (0.2012)^2} \quad \approx 0.83 \text{ keV}. \tag{2.20}$$

2.4.2 ^{60}Co vs ^{22}Na as calibration sources

The data from ^{60}Co were used for calibration. The acquired linear equation was applied to ^{22}Na, ^{137}Cs and the background. The same method was used but with ^{22}Na as a source, the peak positions were then compared to *nndc* [7] tabulated values, and it was concluded that ^{22}Na has its calibrated peaks closer to the tabulated values, and was therefore used as the calibration source.

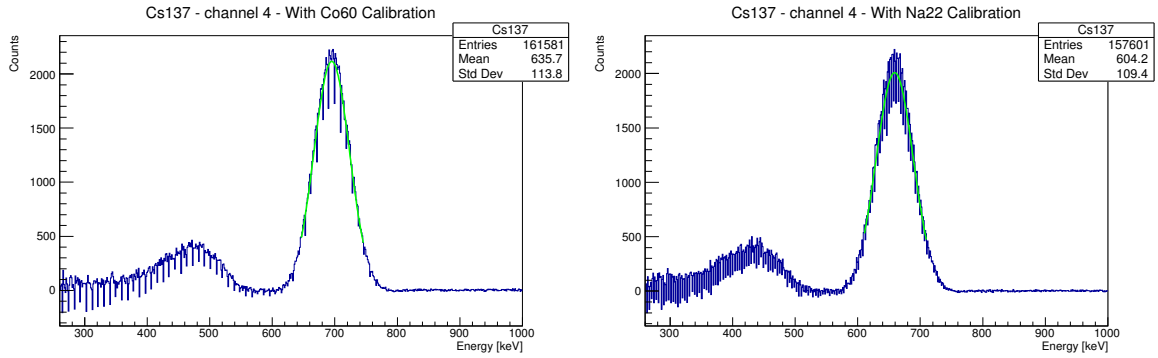

Figure 2.12: Comparison between using ^{60}Co or ^{22}Na as a calibration source, in this case on ^{137}Cs.

Figure 2.12 and tables 2.1 & 2.2 reconfirm that ^{22}Na is the most accurate as a calibration source. The left figure in figure 2.12 shows a cesium spectrum calibrated with ^{60}Co, to the right is the same cesium spectrum but calibrated with ^{22}Na. One can see on the plot and in the tables that when using the ^{60}Co as a source the cesium peak is slightly shifted from the expected ^{137}Cs peak value (661.657 keV). This is partly due to the ^{22}Na peaks being further away from each other compared to ^{60}Co, as mentioned above.

Table 2.1: Calibration with ^{60}Co and the tabulated values from *nndc* [7]. Note that ^{40}K is the room background.

Source	**Calibrated values [keV]**		**nndc tabulated values [keV]**	
	1:st peak	**2:nd peak**	**1:st peak**	**2:nd peak**
^{22}**Na**	541.332 ± 0.108	1274.39 ± 0.462	511.1 ± 0.003	1274.537 ± 0.007
^{60}**Co**	1173.61 ± 0.31	1332.34 ± 0.32	1173.228 ± 0.003	1332.492 ± 0.004
^{137}**Cs**	695.151 ± 0.103		661.657 ± 0.003	
^{40}**K**	1460.73 ± 0.44		1460.820 ± 0.005	

Table 2.2: Calibration with ^{22}Na and the tabulated values from *nndc* [7]. Note that ^{40}K is the room background.

Source	**Calibrated values [keV]**		**nndc tabulated values [keV]**	
	1:st peak	**2:nd peak**	**1:st peak**	**2:nd peak**
^{22}**Na**	511.04 ± 0.11	1274.76 ± 0.52	511.1 ± 0.003	1274.537 ± 0.007
^{60}**Co**	1169.51 ± 0.34	1334.79 ± 0.35	1173.228 ± 0.003	1332.492 ± 0.004
^{137}**Cs**	659.54 ± 0.20		661.657 ± 0.003	
^{40}**K**	1467.8 ± 0.6		1460.820 ± 0.005	

Table 2.3: Propagation of uncertainties using ^{60}Co and ^{137}Cs sources, while k and m are obtained from the linear equation used in the calibration. ∂k and ∂m denote the uncertenties of k and m respectively.

Calibrated with ^{60}Co	k = 0.253278	$\partial k = \pm 0.000709$
	m = 1252.8600	$\partial m = \pm 0.2230$
	$\sum_{\textbf{uncertainty}}$	1.673751 keV

In Tables 2.3 and 2.4, we can observe that the k values of both calibrations (^{60}Co & ^{22}Na) are close to each other (with a difference of approximately 1.06 %), as well as ∂k and ∂m values. However when we come to the total uncertainty, there is a difference between them. During sodium calibration, the total uncertainty is approximately 0.83 keV while the cobalt calibration is 1.67 keV, which is twice as much.

Table 2.4: Propagation of uncertainties using ^{22}Na and ^{137}Cs sources, while k and m are obtained from the linear equation used in the calibration. ∂k and ∂m denote the uncertenties of k and m respectively.

Calibrated with ^{22}Na	k = 0.263842	$\partial k = \pm 0.000167$
	m = 892.8185	$\partial m = \pm 0.2414$
	$\sum_{\textbf{uncertainty}}$	0.827596 keV

2.4.3 Peak position dependency

There are many factors that affect the peak position but the major factor is the ROOT's own Tspectrum. The factors are tested to prove that Tspectrum is the main contributor to affect the peak position. The following data presents how the peak position varies when a factor changes and the other parameters are kept constant, namely the used γ energies, the bin width of the histogram, integral starting and end points, and finally the start and end points for the fit. The conclusion is that the bin size affects the peak position by a maximum value of 0.6 keV.

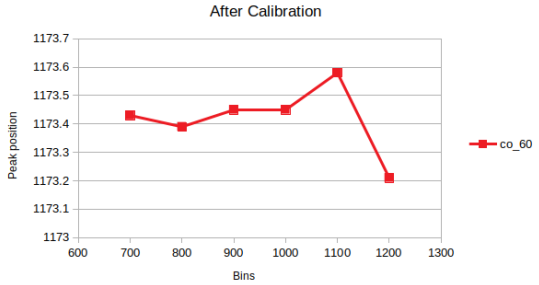

(a) Plot of how difference bins in the script affect the peak position.

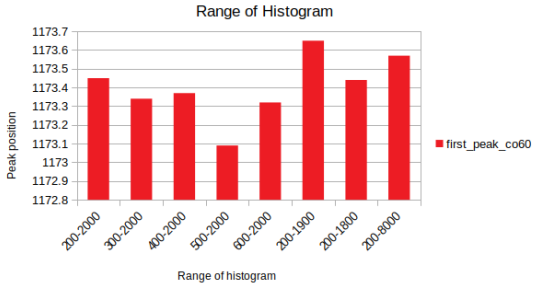

(b) Plot of how the range of the histogram in the script affect the peak position.

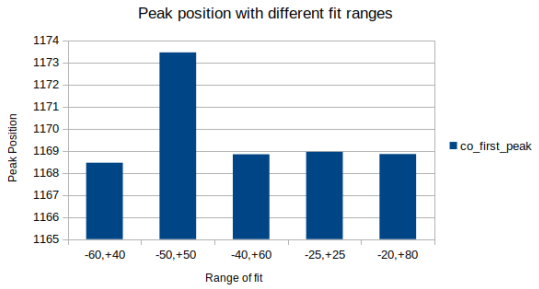

(c) How the range of fits affect the peak position. The fits is defined as how many energy channels are taken before(-) and after (+) the peak maximum (where the derivative is zero.) The fit before calibration used -50,+50 and as seen in the figure, the fit becomes best when uses -50 +50 after calibration too.

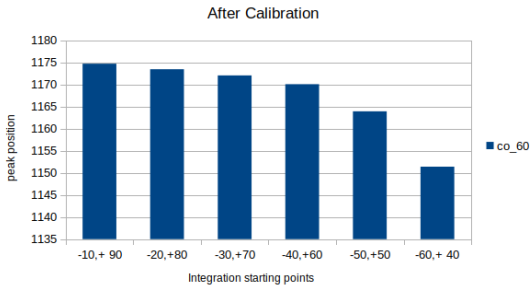

(d) How the integration starting points from the peak affect the peak position.

Figure 2.13: An illustration of how different factors a):the number of bins in the spectrum, b):Different ranges of the spectrum, c):The ranges of how symmetric or asymmetric the fit is done around the peak and finally d):Different limits for the pulse affect the peak position.

3
Results & Analysis

In this chapter the results from measurements for different crystals and different parameters such as different positions and high voltages are presented.

3.1 Energy resolution with different voltages

Using a ^{22}Na source and with different PMT voltages the resolution was studied. The source was placed on the top position for channels 0 and 2, and the low positions for channels 4 and 6, see Fig. 2.6. The resolution for $LaBr_3$ is given in Fig. 3.1.

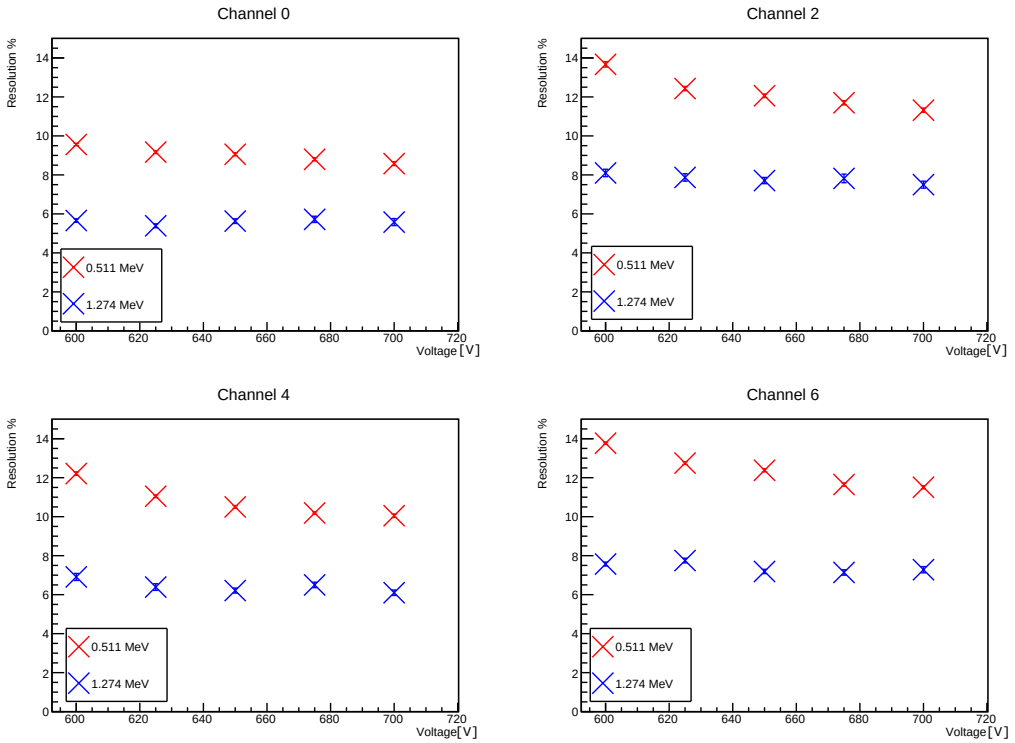

Figure 3.1: The resolution for different PMT voltages on all four $LaBr_3$ crystals using a ^{22}Na source.

As the energy resolution in % is calculated by $2.35\sigma/\bar{x}$ it is naturally to see a better resolution at peak 2 (1274 keV), as the $\bar{x}$ is higher for peak 2. There is similar behavior for all the channels, but channel 0 stands out with the best resolution. For peak 2 there is no major change in resolution when higher voltages is applied.

It can be seen from Figure 3.1 that our measurement has for the ^{22}Na like at 511.1 keV, 600 V, for crystal 1 (channel 0) a resolution of 9.5%, for crystal 2 (channel 2) a resolution of 13.5%, for crystal 3 (channel 4) 12.25% and crystal 4 (channel 6) 13.75%.
The same procedure was repeated for the $LaCl_3$ crystals. The ^{22}Na source was placed 10 cm from the front-face of the detector.

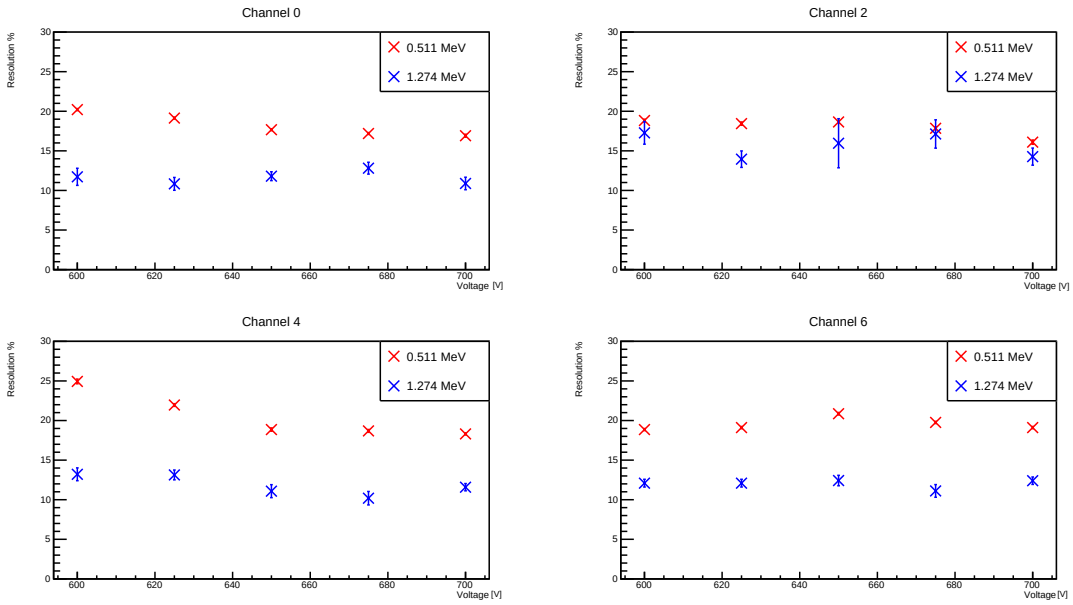

Figure 3.2: The resolution for different PMT voltages on all four $LaCl_3$ crystals using a ^{22}Na source.

It can be seen in the Figure below 3.2, that for $LaCl_3$ at the same keV and voltage the resolution was for crystal 1, 20%, crystal 2, 18.5%, crystal 3, 25% and crystal 4, 19%.

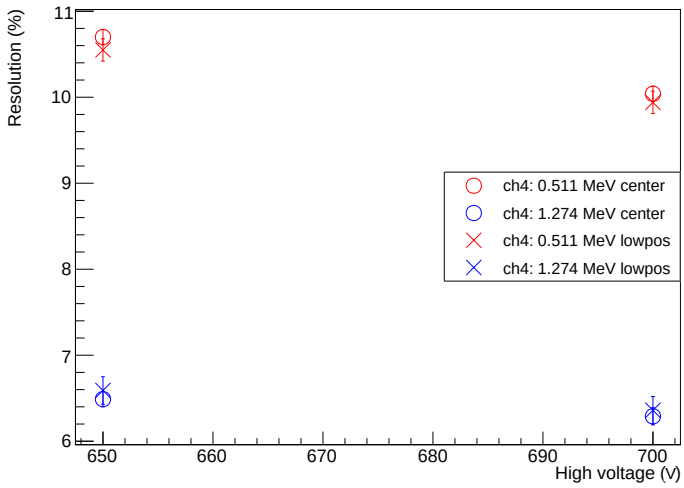

Figure 3.3: The resolution versus different PMT voltages for $LaBr_3$ for channel 4 where the source was placed centered versus the low position, see Figure 2.6. Crosses represent low positions and circles centered positions.

3.2 Calibration

The following four tables 3.1, 3.3, 3.5 and 3.7 represent the four crystals calibrated with the ^{22}Na source. The tables show how much the measured peak energies differ from the tabulated *nndc* values [7]. Tables 3.2, 3.4, 3.6 and 3.8 represents the slope (k) and offset (m) values as well as their uncertainties from the linear equation used in the calibration. Using equations (2.15) and (2.17) we can calculate ∂k and ∂m, the uncertainties for the slope and offset, respectively. Thereafter we have the possibility to calculate the total uncertainty by using equation (2.18).

Table 3.1: Calibration with ^{22}Na of Channel 0. Columns to the right titled "nndc tabulated values" represents the tabulated energy values from *nndc* [7], while to the left columns titled "Calibrated values" correspond to the calibrated energy values using ^{22}Na as a source. Note that ^{137}Cs and ^{40}K have only one γ-peak and that the ^{40}K peak originates from room background.

Source	**Calibrated values [keV]**		**nndc tabulated values [keV]**	
	1:st peak	**2:nd peak**	**1:st peak**	**2:nd peak**
^{22}**Na**	510.341 ± 0.142	1275.65 ± 0.59	511.1 ± 0.003	1274.537 ± 0.007
^{60}**Co**	1173.56 ± 1173.56	1338.24 ± 0.39	1173.228 ± 0.0030	1332.492 ± 0.004
^{137}**Cs**	666.149 ± 0.093		661.657 ± 0.003	
^{40}**K**	1460.82 ± 1.35		1460.820 ± 0.005	

Table 3.2: Propagation of uncertainties using ^{22}Na and ^{137}Cs sources, while k and m are obtained from the linear equation used in the calibration. ∂k and ∂m denote the uncertenties of slope and the offset respectively.

Channel 0	k = 0.153260	$\partial k = \pm 0.000245$
	m = 892.8185	$\partial m = \pm 0.611255$
	$\sum_{\textbf{uncertainty}}$	0.720613 keV

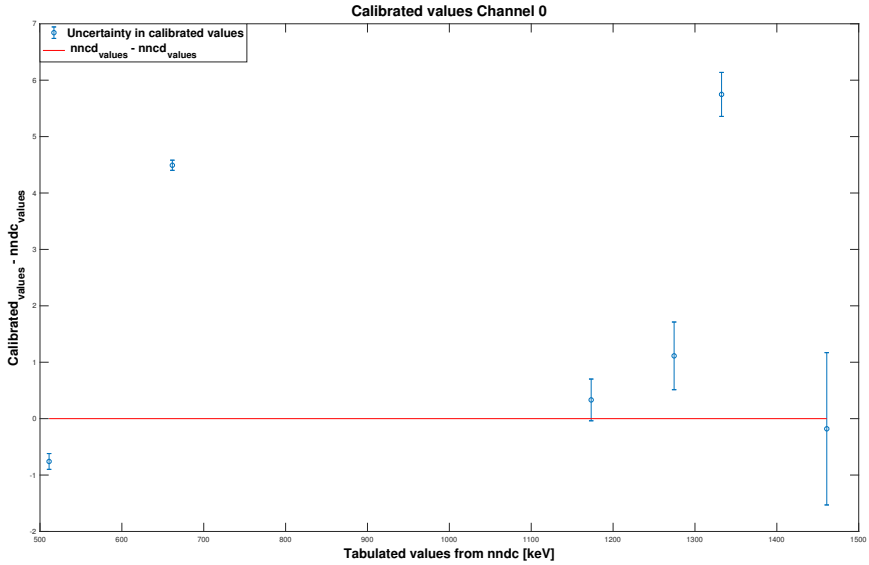

Figure 3.4: This figure shows calibrated values from channel 0. The red line corresponds to the tabulated values from *nndc* [7]. Plotted are also the differences between the calibrated- and tabulated values from *nndc* [7] on the y-axis as a function of tabulated values itself.

The same approach is also applied to the following Figures 3.5, 3.6, and 3.7, which corresponds to the remaining channels 2, 4 and 6 (crystal 2,3 and 4)

Table 3.3: Calibration table with ^{22}Na as a γ-source on channel 2 (crystal 2). As before the right column is the tabulated values from *nndc* [7], and the right column is the calibrated peak positions for ^{22}Na,^{60}Co,^{137}Cs and ^{40}K

Source	**Calibrated values [keV]**		**nndc tabulated values [keV]**	
	1:st peak	**2:nd peak**	**1:st peak**	**2:nd peak**
^{22}**Na**	510.44 ± 0.26	1274.63 ± 1.48	511.1 ± 0.003	1274.537 ± 0.007
^{60}**Co**	1169.53 ± 0.78	1335.38 ± 0.10	1173.228 ± 0.0030	1332.492 ± 0.004
^{137}**Cs**	665.208 ± 0.170		661.657 ± 0.003	
^{40}**K**	1508.95 ± 2.87		1460.820 ± 0.005	

Table 3.4: Total uncertainty of a ^{137}Cs when using ^{22}Na as calibration source. The value k, m, ∂k and ∂m is obtained from the linear equation and the total uncertainty is found with equation 2.18

Channel 2	k = 0.247809	$\partial k = \pm 0.000484$
	m = 892.8185	$\partial m = \pm 0.745165$
	$\sum_{\textbf{uncertainty}}$	0.887517 keV

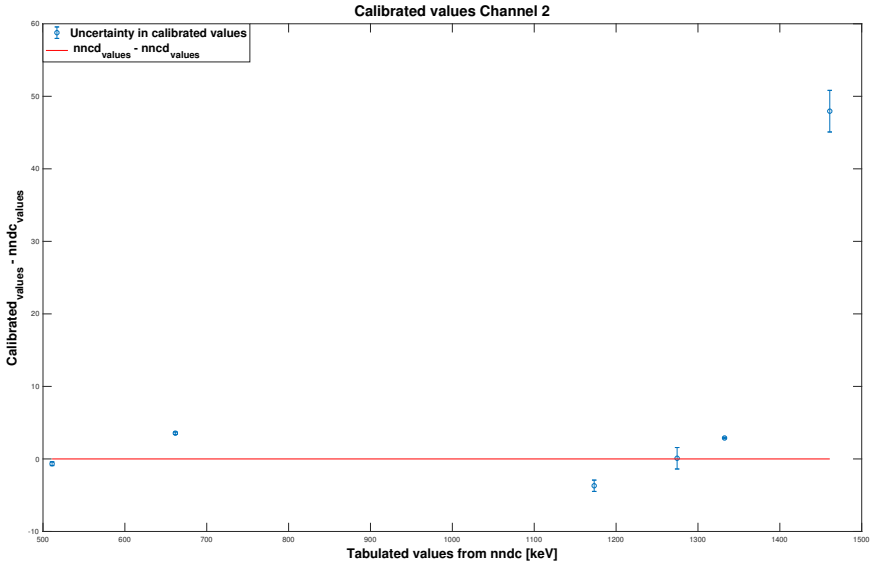

Figure 3.5: In this figure we see the differences between the tabulated values from *nndc* [7] and the calibrated values with ^{22}Na, where as the red line represented the expected values and the blue dots represents the calibrated value for all the peaks.

Table 3.5: Calibrated peak positions for Channel 4 (crystal 3) when using ^{22}Na as a source. Calibrated values given in *keV* for all the peaks in the left column and tabulated values in the right. Note that ^{137}Cs and ^{40}K only has 1 peak where as the ^{60}Co and ^{22}Na has two.

Source	**Calibrated values [keV]**		**nndc tabulated values [keV]**	
	1:st peak	**2:nd peak**	**1:st peak**	**2:nd peak**
^{22}**Na**	511.04 ± 0.11	1274.76 ± 0.52	511.1 ± 0.003	1274.537 ± 0.007
^{60}**Co**	1169.51 ± 0.34	1334.79 ± 0.35	1173.228 ± 0.0030	1332.492 ± 0.0004
^{137}**Cs**	659.54 ± 0.20		661.657 ± 0.003	
^{40}**K**	1467.80 ± 0.64		1460.820 ± 0.005	

Table 3.6: The linear parameters and their uncertainties from the calibration when using ^{22}Na as a source applied on ^{137}Cs for Channel 4 (crystal 3). Also total uncertainty calculated with equation 2.18

Channel 4	k = 0.263842	$\partial k = \pm 0.000167$
	m = 892.8185	$\partial m = \pm 0.241463$
	$\sum_{\mathbf{uncertainty}}$	0.827596 keV

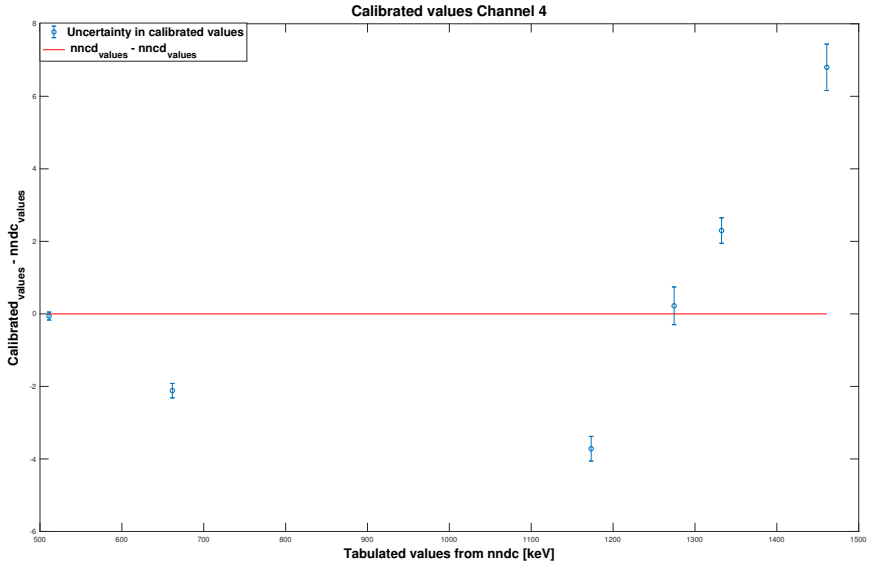

Figure 3.6: The blue dots with error-bars represent the calibrated peak positions while the red line represents the expected values from *nndc* [7]. The peak positions are from ^{22}Na, ^{60}Co, ^{137}Cs and finally ^{40}K. Note this is for channel 4 (crystal 3).

Table 3.7: Calibrated peak positions for different isotopes when ^{22}Na was used as calibration source. Column to the right is tabulated energy values from *nndc* [7]. Note this is for channel 6 (crystal 4).

Source	**Calibrated values [keV]**		**nndc tabulated values [keV]**	
	1:st peak	**2:nd peak**	**1:st peak**	**2:nd peak**
^{22}**Na**	511.141 ± 0.115	1274.74 ± 0.49	511.1 ± 0.003	1274.537 ± 0.007
^{60}**Co**	1170.64 ± 0.48	1336.25 ± 0.54	1173.228 ± 0.003	1332.492 ± 0.004
^{137}**Cs**	664.154 ± 0.206		661.657 ± 0.003	
^{40}**K**	1487.43 ± 0.91		1460.820 ± 0.005	

Table 3.8: The linear values from the calibration with ^{22}Na applied on ^{137}Cs. The uncertainties (∂k, ∂m) of the linear values and the total uncertainty is also presented.

Channel 6	k = 0.323766	$\partial k = \pm 0.000199$
	m = 892.8185	$\partial m = \pm 0.234227$
	$\sum_{\textbf{uncertainty}}$	0.824748 keV

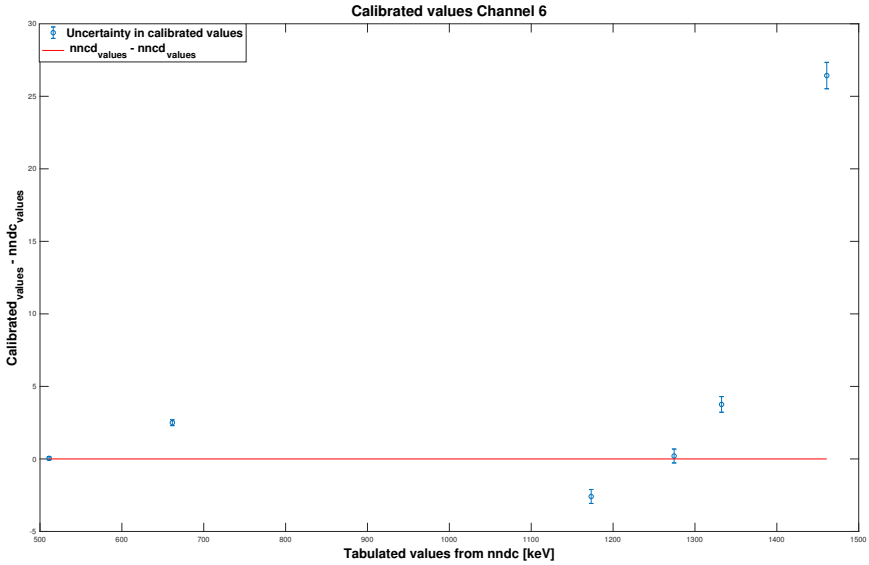

Figure 3.7: For channel 6 (crystal 4), the figure present how much the calibrated peak positions differ from the expected tabulated values *nndc* [7].

In this work, calibrated and measured values differed significantly. The larger the energy difference between the two peaks used in calibration the smaller the difference to nndc values. The problem that a linear calibration alone is not sufficient remains.

3.3 Position dependence

During all position dependence measurements ^{137}Cs was used as a source. ^{137}Cs has a peak at 662 keV. In Figure 3.8 measurements were done with the source along the "centerline" between crystals 1 and 2. The two figures on the left are position dependence for crystal 1 (channel 0), were $LaBr_3$ is the upper figure and $LaCl_3$ is the lower figure, and the same for crystal 2 (channel 2) on the right side. The x-axis indicates the distance from the front-face of the crystal and y-axis the peak position divided by the mean. The mean is defined as the mean of all the peaks positions that are included in each individual figure.

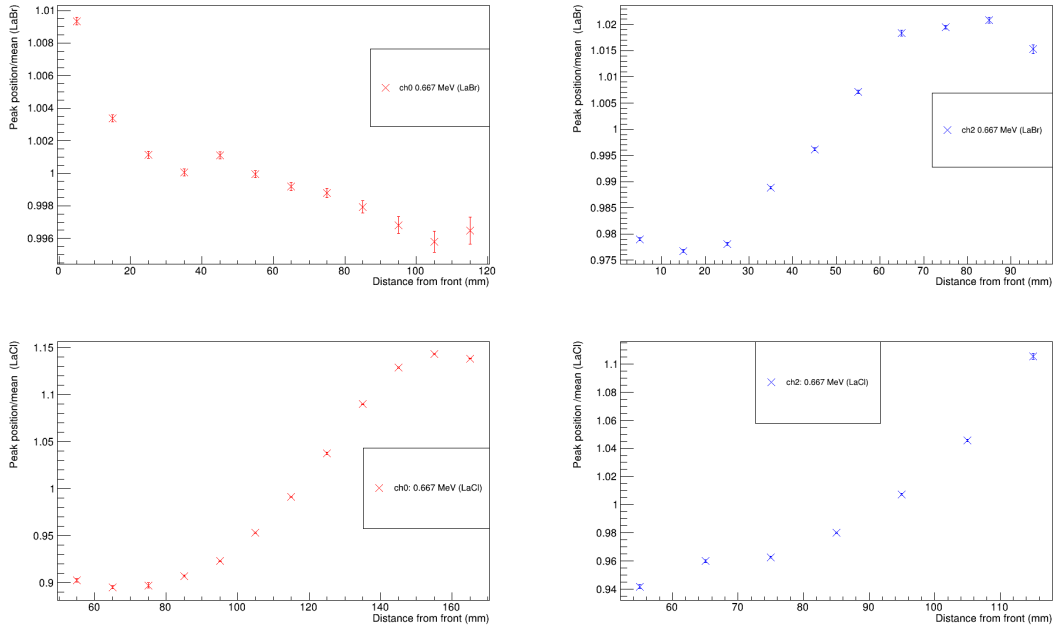

Figure 3.8: The picture presents the position dependence for crystals 1 and 2. The left side presents crystal 1 with $LaBr_3$ on top and $LaCl_3$ on the bottom. The right side shows the same, but for crystal 2.

The same procedure resulted in figure 3.9 for crystal 3 (channel 4) and 4 (channel 6).

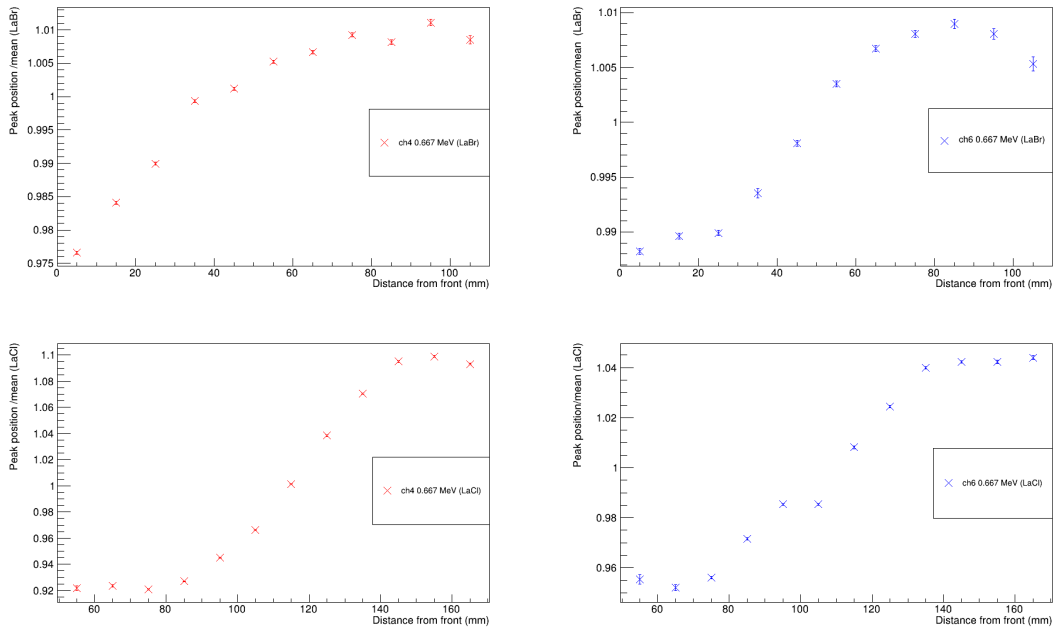

Figure 3.9: The picture presents the position dependence for crystals 3 and 4, the left side is crystal 3 with $LaBr_3$ on top and $LaCl_3$ right side is the same but for crystal 4

By observing Figure 3.8 & 3.9 one can see that the behavior for all the crystals is the same (exponential growth) except for the $LaBr_3$ part of crystal 1 (channel 0). However the difference of the peak positions are greater in the other crystals, more specifically a total difference of less than 0.5 % in crystal 1 and approximately 3 % in the other three crystals. If we instead look at the $LaCl_3$ the behavior is the same for all of the crystals. The change of peak position differs the most in crystal 1 (25%) and the least in crystal 4 (8%). This is odd since the $LaBr_3$ part of crystal 1 was clearly the best as far as the energy resolution is concerned.

Since the behaviour in the $LaBr_3$ part of crystal 1 was different from the other crystals, the measurement was repeated. The blue markers in Figure 3.10 are indicating the peak positions (divided by the mean) of the repeated and the red circles show the original measurement.

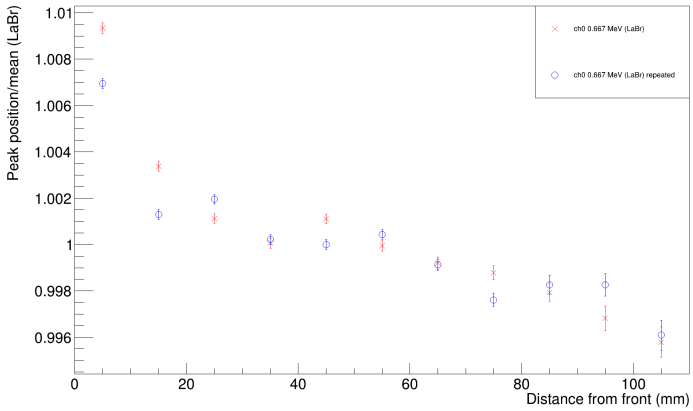

Figure 3.10: Measurements of channel 0 on $LaBr_3$ part of the crystal. The x-axis represents the distance from front and the y-axis gives peak positions divided by the mean value of all the peak positions.

The measurement for Figure 3.10 was mainly done because of the odd behavior of crystal 1. This measurement was a indication that this result can be replicated which is good because then we can also clarify that we did not do anything wrong first time around.
In Figure 3.11 results from the collimator measurements of crystal 1 are plotted together with the same two left figures presented in Figure 3.8, it is added to make it easier to see the correlation between the collimator data points and the "centerline" method. More Collimator points are added in the left figure($LaBr_3$).

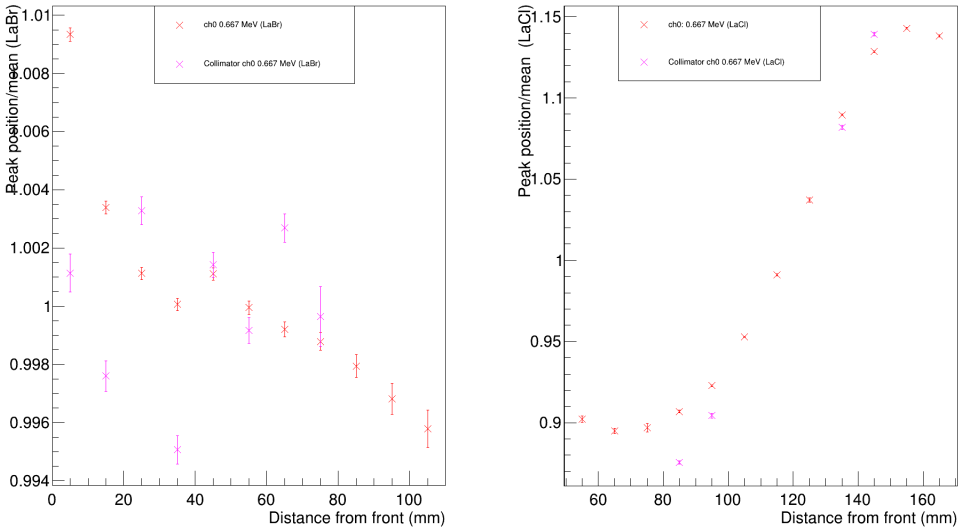

Figure 3.11: The red markers are indicating the measurement without the collimator (same as upper left and bottom left in Figure 3.8) magenta markers are added which represents values when a collimator is used on channel 0. ($LaBr_3$ on the left and $LaCl_3$ on the right)

Moreover Figure 3.11, the collimator data points of the figure $LaBr_3$ did not determine anything (no exponential growth) than the behavior seen earlier in "centerline" method, and we can conclude that this is the typical behaviour of crystal 1. The collimator values in the $LaCl_3$ could be explained, because when using the "centerline" method there is a greater amount of statistics which means that the peak is less pronounced in the spectrum. So when the fit is performed it will be an insignificant change compared to when a collimator is used.

In Fig. 3.12 a measurement over a time window of 16 hours is presented. In this measurement the source was placed on top of the collimator. The collimator was fixed 35 mm from the front face of the sector. During this long measurement it was also possible to determine the peak position dependence for background radiation ^{40}K.

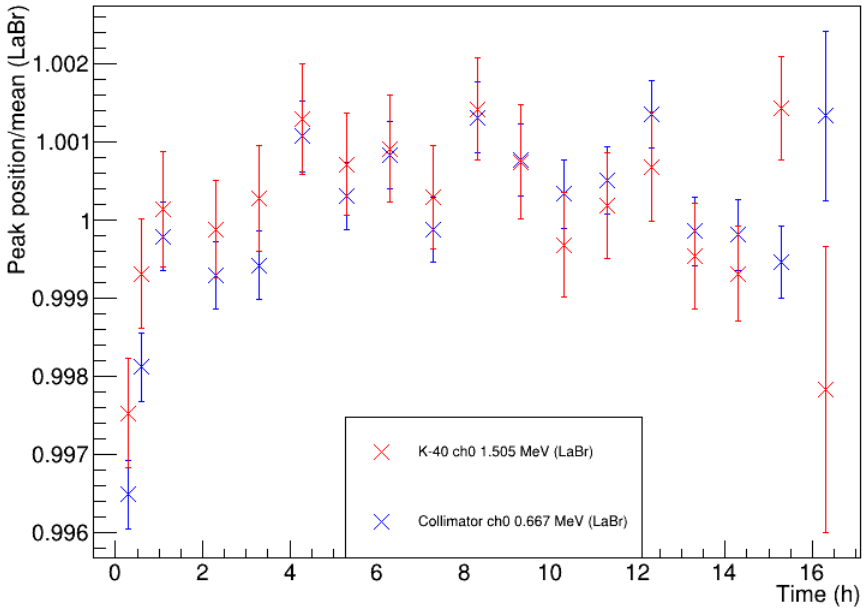

Figure 3.12: Fluctuations of the peak positions of ^{137}Cs and ^{40}K as function of time, for channel 0 (crystal 1). The ^{137}Cs source was placed on top of the collimator and ^{40}K line originates from the room background radiation.

The purpose of Figure 3.12, is to see if there were fluctuations in the electronics. As seen in the figure the first four hour period, the fluctuations seem only to increase and after this period they seem to give a reasonable even distribution. This could mean that the digitizer needs to warm up, and if this is the case it is very frustrating since almost all of the measurements in this project were done in a time window of less than four hours. However, if we ignore the first hours the peak position seems to fluctuate about 0.3%. If we now look back to the position dependence in $LaBr_3$ in crystal 1 one can subtract this electronic difference and this still results in a position dependence but a rather small (0.2%) one.

Figure 3.13 presents the change of peak position in both ^{137}Cs and ^{40}K when the distance is varied and a collimator is used. The distance is varied from the front.

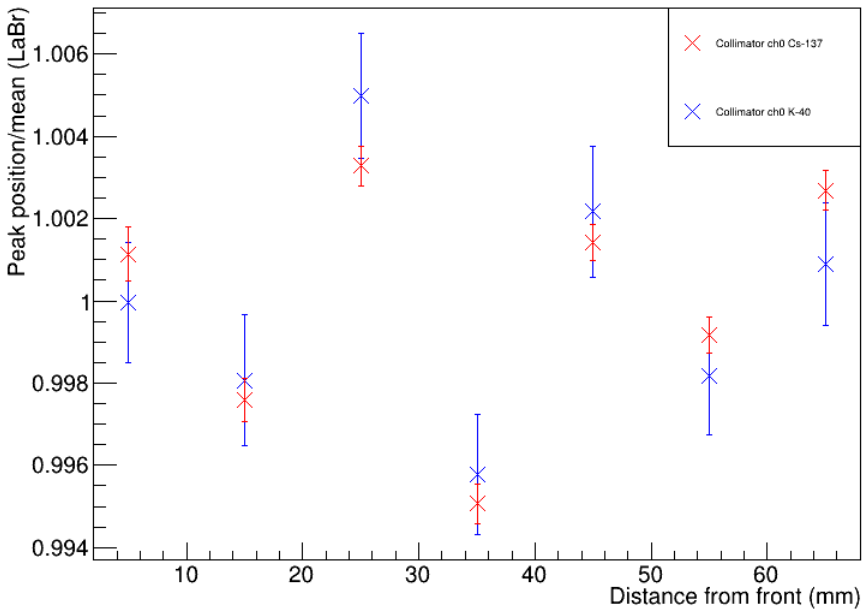

Figure 3.13: Correlation of the ^{137}Cs and ^{40}K when the distances are varied. ^{137}Cs is ontop of the collimator and ^{40}K as the background radiation.

Here again a behaviour where the peaks seem to be dependent on each other (they both move in the same direction) can be seen. Note that the error bars on the ^{40}K line is larger. This is possibly due to the position dependence of the crystal or that the statistical error is larger because of the lower number of counts of background radiation.

4
Discussion

This chapter discuss the results for the energy resolution, calibration and position dependence. Also future improvements are discussed.

4.1 Energy resolution versus different voltages

We expect a better energy resolution when more voltage is applied, the noise before the PMT will also be enhanced but the noise after the PMT will diminish relative to the signal. It can be seen from Figure 3.1 that the resolution levels out at higher voltages.
The previous tests [5] done on CEPA4 demonstrated that the four crystals have a resolution (for γ-rays from a ^{137}Cs source at 661.66 keV) of 3.9% for $LaBr_3$ and 6.5-7% for $LaCl_3$. However our test uses the same electronics as the report "How to lighten Instrumentalist's Life with Electronics" [4] so the results need to be compared to them. The reports state that for 600 V, the resolution for 662 keV is 5.5%. And for 1332 keV with the same parameters the resolution is 3.8%. This is for $LaBr_3$, crystal 1, a resolution which is 1.727 times worse than the previous measurements [4], crystal 2 is 2.45 times worse, crystal 3 is 2.22 times worse and crystal 4 is 2.5 times worse. It could be possible to obtain a better resolution if the source was placed centered on the crystal instead of using the mid position. But this will only have small effect on the resolution as this has been tested, see Figure 3.3. Also larger text files and more data could improve the resolution, however also these will not increase the resolution significant, so that it is impossible for the resolution to reach the TDR values.

4.2 Calibration

A deviation of the calibrated values measured with respect to those expected from nndc can be seen from Figures 3.4, 3.5, 3.6 and 3.7. Channel 0 deviates 6.133keV (table 3.1), channel 2 (table 3.3) deviates 4.48 keV, channel 4 (table3.5) deviates 4.063 keV and channel 6 (table 3.7 deviates 4.301 keV. Compared to the total uncertainties in tables (3.2, 3.4, 3.6 and 3.8), we can seen that the systematic error is larger than the propagation of uncertainty.

Comparing the ^{40}K peak with the other peaks, see table 3.7 one will realize that the other peak energies differ by about 3 keV on average from the *nndc* [7] values. If different crystals would fluctuate by the same amount around the expected values,

then it could be suspected that it depends on the background radiation, and that it is the background that have shifted the peak position. Then this could explain the systematic error problem.

We have found that this detector, unfortunately, has a position dependence on the energy we measure. This means that the ^{40}K peaks we measure are the ones that mostly will end up at the wrong energy, on average. This is because the background radiation impinge on the entire surface of the crystal. In table 3.7 we see that the potassium peak is at 1460.82 ± 1.35097 keV. This is a coincidence since the potassium peak is the peak which is expected to vary the most, because of the position dependence.

Furthermore, since there are fluctuations in the electronics over time, those fluctuations need to be take into consideration. The fluctuations are in the order of a few permil. However since the fluctuations are so small this is not a crucial part of the error.

4.3 Position dependence

The difference in the behaviour of crystal 1 and the other crystals could be discussed as a defect in the scintillator since the same behavior was found when investigating the energy resolution, where as crystal 1 has best resolution for the $LaBr_3$ but in $LaCl_3$ the resolution is the same for all the crystals.

Analyzing the $LaCl_3$ crystals, it seems like the energy dependence becomes constant at the end of the sector. This is speculated to be a problem with light collection, which means that the fraction of scintillated photons that are picked up by the PMT is a lot less than expected. There is also an other possible explanation for this, which is that the crystal is only 15 cm long and in the Figures 3.8 & 3.9 the linear behavior starts around 145 mm. One counter argument against this is that when the γ-source is on top of the crystal ("centerline") the radiation spread against the crystal is almost 180 degrees, which means that there should still be a lot of interactions in the crystal even though the source is placed behind the PMT. There can also be some speculation on the photon transportation, which means that if the photons do not reach the PMT in a straight path but reflect on the surfaces of the scintillator, the reflection could also lead to a light collection problem. The other crucial attribute of the position dependence in the crystal from Figure 3.12 is that the background radiation ^{40}K always follows the behavior of the ^{137}Cs. This means that if the peak of ^{137}Cs increases then the peak of ^{40}K also increases. If this was not the case there would be a critical error in the detector, which indicates that peaks do not shift independently.
The same was investigated in Figure 3.13 and showed that the ^{40}K peak always follows the ^{137}Cs peak. But in this case not over time, but over distance.

4.4 Overview & improvements

In the calibration process, more measurements could be done, for example with the source Europium, ^{152}Eu, as this isotope displays many characterizing peaks, however due to the limited energy resolution of the crystal this would be hard to realise since the crystal could probably not distinguish the different peaks. However since the position dependence had a critical impact on the peak positions one could say it would be better to use background radiation as calibration source, since it has no position dependence (background interact everywhere in the crystal). Longer measurements for background radiations would decrease the statistical error in ^{40}K, which could explain one part of the great error in our calibrated ^{40}K values.

One practical idea to improve the energy resolution is to optimize the script, e.g to have a function where the measured background radiation is subtracted from each spectrum. This way the peaks could be easier determined. This could also be solved by having a lead shield all around the detector, however the impact of this would probably still not meet the criteria of the TDR. And such measurements would take a long time.

Higher voltage on the PMT would not increase the resolution, since the resolution levels out and reaches a maximum when higher voltage is applied.
The collimator could be used on more crystals than only crystal 1, but since the collimator was used on the $LaCl_3$ (crystal 1) and clarified the expected result the same results would probably come out of measurements from crystal 2 and 3.
The results did not meet the any of the requirements so the first idea of further measurements would be to see if the other two sectors that are available at Chalmers would show the same behavior as the sector tested in this report. One property of the crystals that has not been characterized in this study is the time resolution. This property could be measured with cosmic muons and an experimental setup for this is located at Chalmers.

5
Conclusion

The expectation for the measurements of the crystals was that they should match previous measurements done in Ref. [4] with a prototype called CEPA4, however this was not the case. All four crystals are significantly worse than the previous test, crystal 1 (channel 0) however has the best resolution out of the four, but it is still 1.727 times worse than the previous test. (Remember that the resolution compares 511 keV γ-rays in our measurement against 662 keV γ-rays in the previous measurement [4].) The calibration measurements did not either leave a good mark, the background ^{40}K was not close to its correct peak position, the ^{40}K peak position is 1460.82 and crystal 2 (channel 2) ended up at 1508.95 keV see table 3.3, which is a deviation of 3.29%. When different sources were used on the crystal, neither of the four crystals could meet all of the nndc tabulated values (see table 3.3) for the characteristic peak positions of the sources, see Figures 3.4, 3.5, 3.6 and 3.7. The sector that was investigated exhibited a significant position dependence. The $LaBr_3$ part of crystal 1 had the lowest position dependence of its energy signal, which corresponds to a factor of a few permil to 1%. The other crystals showed a greater dependence, with values from 2% to 4.5%. However the $LaCl_3$ exhibit a significantly larger degree of position dependence, where crystal 1 had the worst position dependence of 25%, while the other crystals range between 8% and 18%.

Bibliography

[1] Mikael Mårtensson. (2013) Characterisisation of a $LaBr_3$:$LaCl_3$ Phoswich Array Using 70-230 MeV Protons. Pages 43.

[2] Kenneth S Krane. (1986) Intoductory nuclear physics.

[3] Wikipedia (2019-03-22) Table of nuclides. `https://en.wikipedia.org/wiki/Table_of_nuclides`. Last access 2019-05-28

[4] Giovanni Bruni. (2017) How to lighten Instrumentalist's Life with Electronics. Pages 125

[5] FAIR, NUSTAR. (2015) The R^3B CALorimeter for In Flight detection of rays and high energy charged pArticles. Pages 128

[6] Hamamatsu. (2019) Photomultiplier. `https://www.hamamatsu.com/eu/en/product/optical-sensors/pmt/about_pmts/index.html` Last acess 2019-05-28

[7] NNDC. (2019) Tabulated values. `https://www.nndc.bnl.gov/nudat2/`. Last access 2019-05-28

A

Appendix 1

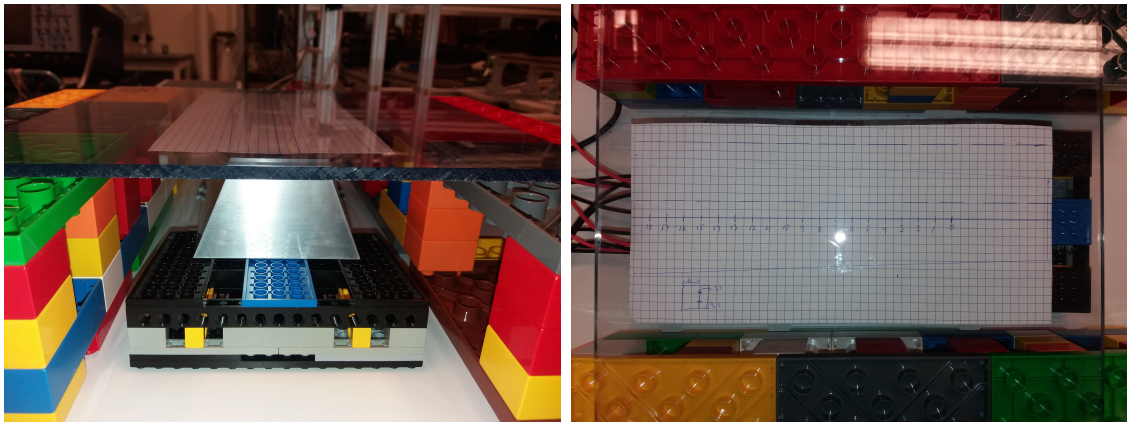

(a) Picture of the detector before the collimator is placed on top the plexiglas.

(b) Paper that indicates where exiting hole of the collimator is focused when the collimator is used.

Figure A.1: Pictures of the setup when the collimator is used. Note that the collimator is not yet placed on the plexiglas in these pictures.